ACS MATERIALS LETTERS

www.acsmaterialsletters.org

Tuning Topology of Two-Dimensional Trifluoromethyl-Functionalized Covalent Organic Framework for Efficient Separation of Isomers

Tian-Tian Ma, Wen-Chao Deng, Hai-Long Qian, Shuting Xu, Cheng Yang, and Xiu-Ping Yan*

Cite This: ACS Materials Lett. 2024, 6, 1616−1622

Read Online

ACCESS | Metrics & More | Article Recommendations | Supporting Information

ABSTRACT: The advantages of designability, functionalizability, and tailorability makes covalent organic frameworks (COFs) promising for separation application. Here, we propose a strategy to improve the performance of gas chromatography for the separation of isomers by tuning the topology of two-dimensional (2D) COFs. 2,5-Diaminobenzotrifluoride (Pa-CF_3) with trifluoromethyl functional group was selected to condense with biphenyl-3,3′,5,5′-tetracarbaldehyde (BTA) possessing D_{2h} symmetry, and 1,3,5-benzenetricarboxaldehyde (Tb) possessing C_3 symmetry, respectively, to prepare heteropore BTAPa-CF_3 and homopore TbPa-CF_3. The prepared BTAPa-CF_3 has a richer pore structure and higher density of the trifluoromethyl functional group than TbPa-CF_3. The abundant pore sizes of the heteropore structure and dipole forces of the trifluoromethyl functional group gave the BTAPa-CF_3 bonded capillary column better performance than the TbPa-CF_3 bonded capillary column for the separation of hexane, heptane, xylene, chlorotoluene, butylbenzene, and isoamyl acetate isomers with good repeatability. This work provides new idea for designing stationary phases for the separation of isomers from a topological view.

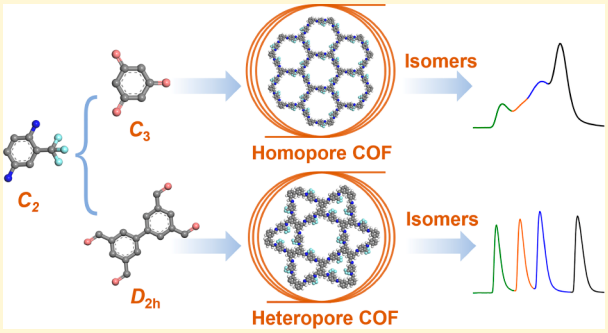

The intriguing properties of tunable structure, large specific surface area, and high thermal and chemical stability enable covalent organic frameworks (COFs), making them promising for use in the chromatographic separation of isomers.[1−5] Due to the similar physicochemical properties of isomers, there is a high demand for the separation ability of the stationary phase.[6,7] Currently, the improvement of the separation performance of COFs stationary phases is usually performed by introducing substituents or selecting suitable building blocks to change the chemical environment of the pores.[2,3,8−11] Moreover, all the COFs currently used as stationary phases are homopores, providing only one single type of pore size. Suitable pore size can enhance subject-object interactions.[12] In view of the limited available monomers, homopore two-dimensional COFs (2D COFs) typically offer apertures larger than 10 Å,[13−16] resulting in poor interaction to the isomers with small molecular diameters, such as hexane (4.3−6.2 Å).[17] Homopore three-dimensional (3D) COFs can give small pore size (∼8 Å), but the availability of 3D COFs is limited, because of the hard-to-synthesize monomers.[10,18,19] Therefore, it is necessary to introduce rich pore structures into 2D COFs for the improvement of the separation of isomers.

Modulating the topology of COFs is expected to improve the separation performance of COFs as the properties of the COFs are closely related to their pore sizes and environment. The topological design of COFs can be achieved by combining building blocks of different sizes and specific symmetries.[20] Heteropore COFs are a type of COF with different sizes and different topologies of pores periodically distributed in the same polymeric structure.[21] Conventional homopore COFs have a uniform pore structure, whereas heteropore COFs possess various pore structures and functional group densities.[21−24] The special properties of heteropore COFs give them potential in the field of separation. However, heteropore COFs have not been applied as stationary phases for chromatographic separation so far.

Received: January 23, 2024
Revised: March 17, 2024
Accepted: March 19, 2024

https://doi.org/10.1021/acsmaterialslett.4c00166
ACS Materials Lett. 2024, 6, 1616−1622

Here, we report the fabrication of 2D COFs with different topologies (heteropore and homopore) to investigate the effect of the topology on the gas chromatographic separation of the isomers. Biphenyl-3,3′,5,5′-tetracarbaldehyde (BTA) and 1,3,5-benzenetricarboxaldehyde (Tb) with different symmetries are chosen as ligands to react with 2,5-diaminobenzotrifluoride (Pa-CF_3) for the synthesis of COFs BTAPa-CF_3 and TbPa-CF_3 with different topologies, respectively (Figure 1).

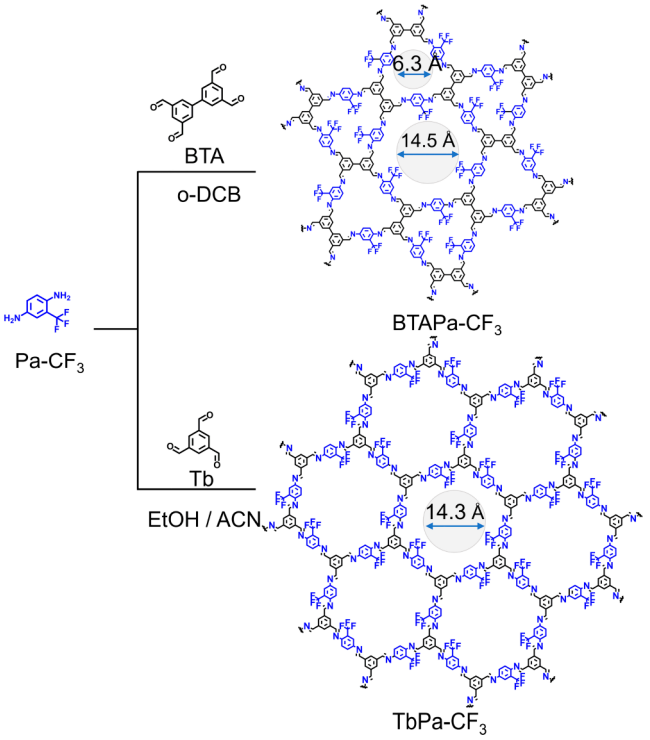

Figure 1. Schematic for the synthesis of 2D COFs BTAPa-CF_3 and TbPa-CF_3 with different topologies.

The trifluoromethyl functional group is introduced into the COFs to enhance the dipole force for the effective improvement of separation.[25] Moreover, TbPa-CF_3 is designed with a pore size similar to that of the larger pore in BTAPa-CF_3 to show the role of the smaller pore in heteropore BTAPa-CF_3 in separation. COF-bonded capillary columns are fabricated by covalent growth of BTAPa-CF_3 and TbPa-CF_3 on the inner wall of capillary columns. The separation performance of the as-prepared capillary columns is investigated to explore the effect of topology on separation. This work provides a new idea for designing stationary phases for the separation of isomers from a topological view.

The designed COFs TbPa-CF_3 and BTAPa-CF_3 were prepared by optimizing the synthesis conditions (solvent composition, reaction temperature, and time). To facilitate subsequent preparation of COF-bound capillary column, both crystallinity and dispersibility were taken into account for the optimization of the synthesis conditions. As a result, TbPa-CF_3 with a yield of 73% was prepared in the mixture of EtOH/ACN/6 mol L^{-1} HAc (6:1.5:1, v:v:v, 1.7 mL) at room temperature for 72 h (Figures S1 and S2, Table S1). For COF BTAPa-CF_3, screening of the solvent components did not yield a solvent system for the good dispersion of BTAPa-CF_3 during the synthesis. Therefore, highly crystalline BTAPa-CF_3 with a yield of 60% was synthesized in the mixture of *o*-DCB/6 mol L^{-1} HAc (5:1, v:v, 1.2 mL) at 120 °C for 48 h (Figures S3 and S4, Table S2).

The crystallinity of the prepared COFs was characterized by X-ray diffraction (XRD) (Figure 2a). BTAPa-CF_3 gave

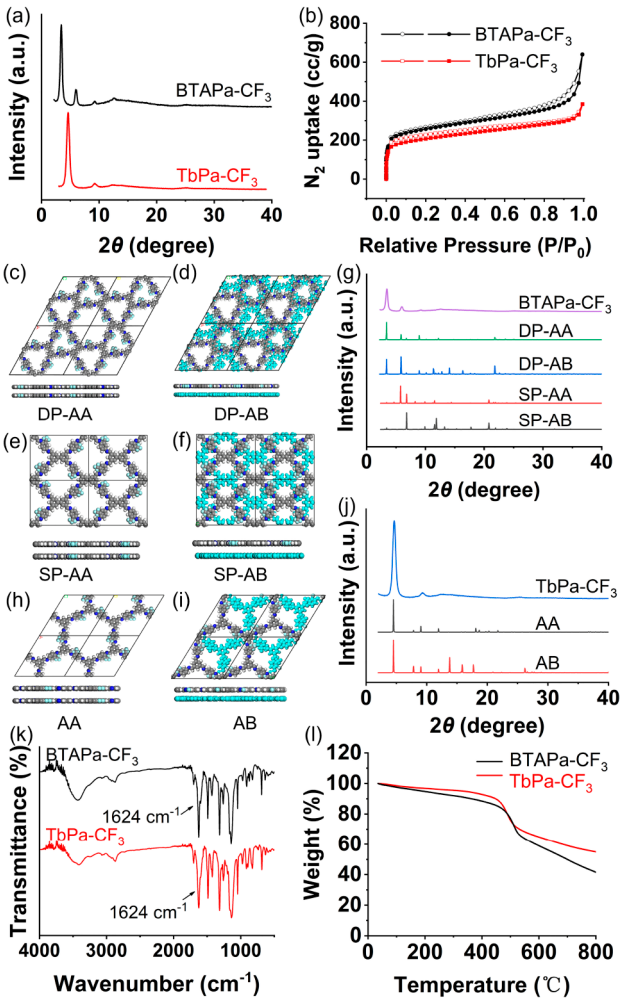

Figure 2. Characterization of BTAPa-CF_3 and TbPa-CF_3. (a) XRD patterns; (b) nitrogen adsorption−desorption isotherms; (c) DP-AA eclipsed unit cell; (d) DP-AB staggered unit cell; (e) SP-AA eclipsed unit cell; (f) SP-AB staggered unit cell of BTAPa-CF_3; (g) comparison of the experimental XRD pattern of BTAPa-CF_3 with the simulated patterns of BTAPa-CF_3 for the DP-AA eclipsed, DP-AB staggered, SP-AA eclipsed, and SP-AB staggered models; (h) AA eclipsed unit cell and (i) AB staggered unit cell of TbPa-CF_3; (j) comparison of the experimental XRD pattern of TbPa-CF_3 with the simulated patterns of TpPa-CF_3 for the AA eclipsed and AB staggered models; (k) FT-IR spectra; (l) TGA curves.

characteristic diffraction peaks at 3.4° and 6.0° for the (100) and (110) facets, respectively, while TbPa-CF_3 exhibited a characteristic diffraction peak at 4.5° for the (100) facet. The porosity of BTAPa-CF_3 and TbPa-CF_3 was determined by nitrogen adsorption−desorption experiments (Figure 2b). Interestingly, two pore sizes of 5.9 and 11.4 Å were observed for BTAPa-CF_3, demonstrating that the prepared material possessed a heteropore structure (Figure S5a). The pore size of TbPa-CF_3 was mainly distributed at 11.0 Å, similar to the larger pore of BTAPa-CF_3 (11.4 Å) (Figure S6a). The above pore sizes are close to the theoretical values estimated by Multiwfn for BTAPa-CF_3 (6.3 and 14.5 Å) and TbPa-CF_3

https://doi.org/10.1021/acsmaterialslett.4c00166
ACS Materials Lett. 2024, 6, 1616−1622

(14.3 Å).[26] Meanwhile, the Brunauer−Emmett−Teller (BET) surface areas of BTAPa-CF_3 and TbPa-CF_3 were determined to be 953 and 762 $m^2\ g^{-1}$, respectively, with pore volumes of 0.772 and 0.484 $cm^3\ g^{-1}$, respectively (Figures S5b and S6b).

The different pore properties of BTAPa-CF_3 and TbPa-CF_3 encouraged us to further investigate the crystalline structure of the COFs by Material Studio 7.0. The combination of D_{2h} (BTA) and C_2 (Pa-CF_3) symmetric monomers is anticipated to generate two kinds of framework structures: single pore (SP) and dual pore (DP). Meanwhile, both of the SP and DP structures exhibit two possible stacking models: staggered (AB) and eclipsed (AA). Therefore, the DP-AA, DP-AB, SP-AA, and SP-AB structure models of BTAPa-CF_3 were constructed (Figure 2c−f). The corresponding XRD patterns were simulated by a power diffraction module. The experimental XRD pattern of BTAPa-CF_3 was more consistent with the simulated one for the DP-AA model featuring Kagome topology (Figure 2g). Based on the XRD pattern and pore size distribution, the as-prepared BTAPa-CF_3 was confirmed to be an AA stacking heteropore structure. Then, the DP-AA model of BTAPa-CF_3 was refined by using the Pawley refinement to obtain cell parameters: space group of $P\bar{6}$, $a = b = 29.6695$ Å, $c = 4.0474$ Å, $\alpha = \beta = 90°$ and $\gamma = 120°$ with $R_{wp} = 5.39\%$ and $R_p = 4.02\%$ (Figure S7, Table S3). Considering the symmetry of the monomers (C_3 for Tb and C_2 for Pa-CF_3), two possible stacking models (AA and AB) were constructed for TbPa-CF_3 (Figures 2h and 2i). The XRD data obtained from the experiment reproduced the simulated XRD pattern of the AA eclipsed structure (Figure 2j). Moreover, only one type of pore size was given by TbPa-CF_3. The results corroborate that TbPa-CF_3 is an AA stacking homopore structure with hexagonal topology. After refinement by the powder diffraction module, the cell parameters of TbPa-CF_3 are as follows: space group of $P\bar{6}$, $a = b = 22.0246$ Å, $c = 4.8722$ Å, $\alpha = \beta = 90°$, and $\gamma = 120°$ with $R_{wp} = 3.27\%$ and $R_p = 2.36\%$ (Figure S8 and Table S4).

The formation of the COFs BTAPa-CF_3 and TbPa-CF_3 was further confirmed by Fourier transform-infrared spectroscopy (FT-IR) (Figure 2k). The appearance of the C═N characteristic peak at 1624 cm^{-1} for BTAPa-CF_3, along with the decrease of the C═O characteristic peak at 1694 cm^{-1} for BTA proved the occurrence of Schiff base reaction (Figure S9). Similarly, the successful preparation of TbPa-CF_3 was verified by the reduction of the C═O characteristic peak at 1696 cm^{-1} for Tb, and the emergence of the C═N characteristic at 1624 cm^{-1} for TbPa-CF_3 (Figure S10).

Scanning electron microscopy (SEM) images show that both BTAPa-CF_3 and TbPa-CF_3 were irregularly spherical (Figures S11 and S12). Since the stationary phases of gas chromatography are often utilized at high temperature, the thermal stability of BTAPa-CF_3 and TbPa-CF_3 was examined by thermogravimetric analysis (TGA). The results showed that both of the COFs were stable at 450 °C (Figure 2l). No obvious change in the XRD pattern and the C═N peak in FT-IR spectra of the BTAPa-CF_3 indicates the good stability of the BTAPa-CF_3 in various solvents of ACN, H_2O, MeOH, THF, EtOH, HCl (0.1 mol L^{-1}) and NaOH (0.1 mol L^{-1}) (Figure S13). Moreover, TbPa-CF_3 was stable in ACN, H_2O, MeOH, THF and EtOH. The significant decrease in the characteristic diffraction peaks and the increase in the C═O characteristic absorption peaks of Tb demonstrate that TbPa-CF_3 was unstable in HCl (0.1 mol L^{-1}) and NaOH (0.1 mol L^{-1}) (Figure S14).

The high thermal stability and superior porosity make BTAPa-CF_3 and TbPa-CF_3 promising stationary phases for gas chromatography. In situ growth method was utilized to fabricate a TbPa-CF_3-bound capillary column due to the good dispersion of TbPa-CF_3 during the synthesis. Briefly, the monomers and reaction solvent were homogeneously mixed and injected into the amino functionalization capillary column. Along with the synthesis of COF, the crystalline TbPa-CF_3 were covalently attached on the inner wall of the capillary column to obtain the TbPa-CF_3-bound capillary column. Due to the insufficient dispersibility of BTAPa-CF_3 in synthetic solvent, the in situ growth method is prone to failure due to clogging of the material in the capillary column. A two-step method was employed to prepare BTAPa-CF_3-bound capillary column.[27] In short, a uniform amorphous polymer layer was first bonded to the interior surface of the capillary column in a suitable solution environment. Then, the amorphous polymer layer was transformed into a crystalline layer in the second step. Detailed preparation steps were provided in the Supporting Information.

The C═N stretching vibration at 1624 cm^{-1} and characteristic diffraction peaks at 3.4° and 6.0° were observed for BTAPa-CF_3 synthesized by the two-step method, indicating the feasibility of the two-step method for the preparation of BTAPa-CF_3 (Figure S15). The crystallinity of the COFs bonded in the capillary columns was characterized by XRD. The consistent XRD patterns demonstrate that the COFs on the inner wall of the capillary columns had the same crystallinity as that synthesized via the solvothermal method (Figure S16a vs Figure 2a). Meanwhile, the bare capillary column, BTAPa-CF_3-bound capillary column and TbPa-CF_3-bound capillary column were characterized by FT-IR. The C═N characteristic absorption peak at 1624 cm^{-1} appeared in the FT-IR spectra of the COFs-bound capillary columns, proving the successful reaction of the amino groups with the aldehyde groups (Figure S16b). SEM images show that both BTAPa-CF_3 and TbPa-CF_3-bound capillary columns had uniform material growth on the inner wall of the capillary columns compared to the bare capillary column (see Figure 3, as well as Figure S17). All of the above results show the successful preparation of COFs-bound capillary columns.

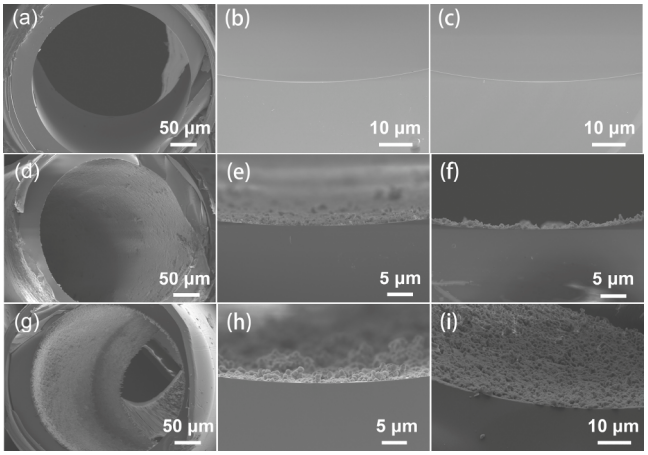

Figure 3. (a−c) SEM images of bare capillary column, (d−f) BTAPa-CF_3-bound capillary column, and (g−i) TbPa-CF_3-bound capillary column from a cross-sectional view.

https://doi.org/10.1021/acsmaterialslett.4c00166
ACS Materials Lett. 2024, 6, 1616−1622

The polarity of the prepared COF stationary phases was evaluated in terms of the McReynolds constants.[28,29] Probes of *n*-BuOH (Y), 1-nitropropropane (U), pyridine (S), 2-pentanone (Z), and benzene (X) were used to determine the McReynolds constants. The average values of McReynolds constants for the BTAPa-CF_3 and TbPa-CF_3 stationary phases were 87 and 88, respectively, showing that both of them were weakly polar stationary phases (Table 1). The introduction of

Table 1. McReynolds Constants of the BTAPa-CF_3-Bound Capillary Column and the TbPa-CF_3-Bound Capillary Column

stationary phase	X	Y	Z	U	S	avg
BTAPa-CF_3	26	96	149	145	20	87
TbPa-CF_3	29	88	164	149	11	88

trifluoromethyl functional groups provided strong proton acceptance and dipole forces, leading to larger values of Z and U for BTAPa-CF_3 and TbPa-CF_3 stationary phases.

Different isomers were used to evaluate the separation performance of the BTAPa-CF_3-bound capillary column and the TbPa-CF_3-bound capillary column to investigate the effect of topology on the separation of isomers. Hexane isomers with molecular diameters (4.3−6.2 Å) similar to the smaller pore (5.9 Å) of BTAPa-CF_3 were chosen to explore the role of the rich pore structure for separation. Meanwhile, separation of hexane isomers is essential for the petrochemical industry to improve the octane numbers (RONs) of gasoline. The multibranched alkanes usually have a higher RON than monobranched alkanes.[30−32] However, effective separation of hexane isomers is challenging because of their chemical inactivity, similar polarizability and boiling point.[18,33] Even so, the prepared BTAPa-CF_3-bound capillary column achieved baseline separation of hexane isomers (2,2-dimethylbutane, 2,3-dimethylbutane, 3-methylpentane, and hexane). Moreover, the larger the molecular diameter, the faster the analyte eluted (Figure 4a). In contrast, the TbPa-CF_3-bound capillary column failed to separate hexane isomers (Figure S18a). The better separation performance of the BTAPa-CF_3-bound capillary column can be attributed to the size exclusion effect provided by the heteropore structure and the dipole force offered by the trifluoromethyl groups.

Xylene isomers with molecular diameters (6.7−7.4 Å) larger than the smaller pore (5.9 Å) of BTAPa-CF_3 were selected to study the effect of functional group density on the separation performance. *p*-Xylene is an indispensable raw material for polyethylene terephthalate, while *m*-xylene and *o*-xylene are present as impurities.[5] Because of the similar boiling points and molecular diameters, the separation of xylene isomers is regarded as one of the seven most challenging separations in the world.[34] The BTAPa-CF_3-bound capillary column enabled the efficient separation of xylene isomers (Figure 4b). In contrast, no baseline separation of xylene isomers was achieved on the TbPa-CF_3-bound capillary column (Figure S18b). Although xylene isomers were unable to enter the smaller pore of heteropore BTAPa-CF_3, the Kagome topology of BTAPa-CF_3 provided a higher density of trifluoromethyl functional groups, leading to a better separation capability.

Diverse isomers were selected to test the versatility of the prepared COF-bound capillary columns. The isomers included position isomers of chlorotoluene, butylbenzene, dichlorobenzene, and nitrotoluene, carbon chain isomers of heptane, ethyl

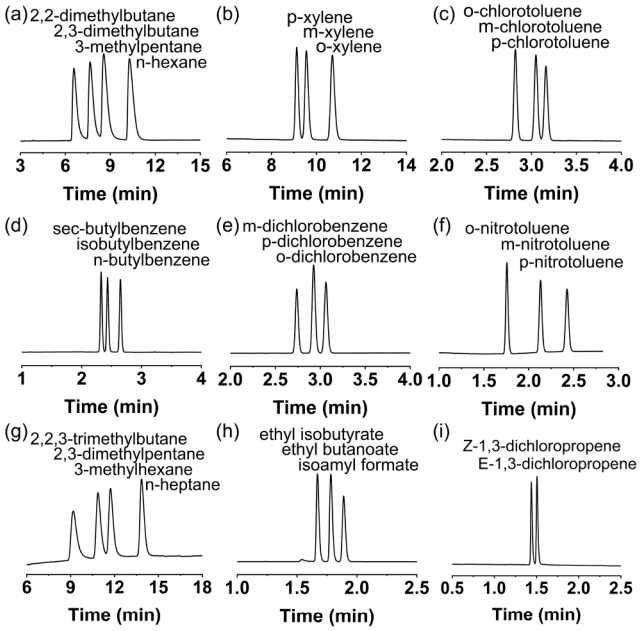

Figure 4. Chromatograms for the separation of isomers on BTAPa-CF_3-bound capillary column: (a) hexane isomers at 90 °C; (b) xylene isomers at 140 °C; (c) chlorotoluene isomers at 190 °C; (d) butylbenzene isomers at 220 °C; (e) dichlorobenzene isomers at 200 °C; (f) nitrotoluene isomers at 250 °C (1.5 mL min^{-1}); (g) heptane isomers at 110 °C; (h) ethyl butanoate isomers at 210 °C; and (i) 1,3-dichlorobenzene isomers at 200 °C. Other separation was performed under a constant flow rate of 1 mL min^{-1}, using N_2 as the carrier gas.

butanoate, and cis−trans isomers 1,3-dichloropropene. All the tested isomers were effectively separated on the BTAPa-CF_3-bound capillary column (see Figures 4c−i, as well as Table S5). However, the TbPa-CF_3-bound capillary column failed to separate the heptane and ethyl butanoate isomers. Isomers of chlorotoluene, butylbenzene, dichlorobenzene, and nitrotoluene were separated on the TbPa-CF_3-bound capillary column, but with a longer time than the BTAPa-CF_3-bound capillary column (Figures S18c−S18i). Except for hexane, heptane, and xylene isomers, other isomers were baseline separated within 3.5 min. Moreover, the mixtures such as *n*-alkanes, alkylbenzene, and esters were baseline-separated on the BTAPa-CF_3-bound capillary column (Figure S19). All of the results indicate the good separation ability of the BTAPa-CF_3-bound capillary column. Bare capillary column was prepared as the control to show the importance of the framework structure of COF in the separation of isomers. The prepared bare capillary column gave no baseline separation of the aforementioned isomers under the optimized conditions (Figure S20), indicating a crucial role of the ordered framework structure of the COF in the separation of isomers.

Molecular docking of COFs and isomers was also performed using AutoDock to predict possible binding conformations. Simulation was carried out with BTAPa-CF_3 and TbPa-CF_3 as receptor molecules and hexane isomers as guest molecules. Compared to the binding conformations of the hexane isomer with homopore COF TbPa-CF_3, the hexane isomers had a tendency to interact with the smaller pore of BTAPa-CF_3 in the heteropore models (Figure S21). The outcomes further confirm the importance of the abundant pore structure of BTAPa-CF_3 in the separation.

https://doi.org/10.1021/acsmaterialslett.4c00166
ACS Materials Lett. 2024, 6, 1616−1622

The thermodynamics for the separation of isomers on the BTAPa-CF_3-bound capillary column were further studied. The relative retention time of the isomers was determined at different temperatures. The capacity factors were calculated to plot the Van't Hoff curves (Figure S22). The good correlation coefficients of the Van't Hoff equations proved that the separation mechanism remained constant over the tested temperature range. According to the calculated entropy change (ΔS), enthalpy change (ΔH), and Gibbs free energy (ΔG), the separation of the isomers was an enthalpy-driven spontaneous process ($\Delta H < 0$, $\Delta S < 0$, and $\Delta G < 0$) (see Table S6).

The separation performance of the BTAPa-CF_3-bound capillary column for the separation of xylene and chlorotoluene isomers was compared with other reported stationary phases. The BTAPa-CF_3-bound capillary column showed shorter separation time or higher resolution than other reported stationary phases, such as MOF-CJ3,[35] COF TpTFMB,[25] COF BtaMth,[36] and ZIF-8@PDMS[37] for the separation of xylene isomers, and P6A-C10,[38] COF TpTFMB,[25] 2D-Zr-BTB-C_6,[39] and $[ZnCl_2L]_2$[40] for the separation of chlorotoluene isomers. The above results demonstrate the good separation ability of the BTAPa-CF_3-bound capillary column (see Tables S7 and S8).

The precision of the prepared BTAPa-CF_3-bound capillary column for the separation of the aforementioned isomers was determined. The relative standard deviations (RSDs) of intraday (n = 5), interday (n = 3), and column-to-column (n = 3) for the retention time were <1.4%, 2.8%, and 5.0%, respectively, and for the peak areas were <3.6%, 5.5% and 8.6%, respectively, indicating the good precision for the separation of isomers on the BTAPa-CF_3-bound capillary column (Table S9).

The good thermal stability of the capillary column can effectively avoid stationary phase loss at high temperature. The prepared BTAPa-CF_3-bound capillary column was aged at a programmed temperature process (from 50 °C to 350 °C, 4 °C min^{-1}) for three times to examine the thermal stability. The column efficiency and capacity factor of the above isomers were reduced by <8.6% and 5.9%, respectively, demonstrating the good stability of the BTAPa-CF_3-bound capillary column (see Table S10).

In conclusion, we have reported the synthesis of 2D COFs BTAPa-CF_3 and TbPa-CF_3 with different topologies and studied the influence of topology on the gas chromatographic separation of the isomers. Since the Kagome topology of the heteropore BTAPa-CF_3 provides a higher density of trifluoromethyl functional groups as well as enriched pore structures to provide multiple pore size effects for different sizes of targets, the BTAPa-CF_3-bound capillary column exhibited a superior separation than the TbPa-CF_3-bound capillary column. Various isomers such as hexane, heptane, xylene, nitrotoluene, 1,3-dichloropropene, chlorotoluene, butylbenzene, dichlorobenzene, and ethyl butanoate were baseline-separated on the BTAPa-CF_3-bound capillary column with good precision. This work provides a new way to design COFs as stationary phases for the separation of isomers.

■ ASSOCIATED CONTENT

Supporting Information

The Supporting Information is available free of charge at https://pubs.acs.org/doi/10.1021/acsmaterialslett.4c00166.

Supplementary methods: chemicals and materials, apparatus for material characterization, synthesis of COFs, details for the pretreatment, amino functionalization and preparation of capillary columns, calculation of thermodynamic parameters and McReynolds Constant. Supplementary figures, including Pawley refinement, FT-IR, SEM, BET surface area, pore size distribution of the prepared COFs BTAPa-CF_3 and TbPa-CF_3; the XRD, FT-IR, and SEM of the prepared COFs-bound capillary columns; the separation performance for the BTAPa-CF_3-bound capillary column, TbPa-CF_3-bound capillary column and bare capillary column; the Van't Hoff plots for isomers separated on the BTAPa-CF_3-bound capillary column, and the molecular docking of COFs and isomers. Supplementary tables, including the yield of the COFs obtained under optimized conditions; fractional atomic coordinates of the COFs; resolution, half-peak width and tailing factor for isomers separation on the BTAPa-CF_3-bound capillary column; thermodynamic parameters, precision and thermal stability of the BTAPa-CF_3-bound capillary column (PDF)

■ AUTHOR INFORMATION

Corresponding Author

Xiu-Ping Yan − *State Key Laboratory of Food Science and Resources, Jiangnan University, Wuxi 214122, China; International Joint Laboratory on Food Safety, Institute of Analytical Food Safety, School of Food Science and Technology, and Key Laboratory of Synthetic and Biological Colloids, Ministry of Education, Jiangnan University, Wuxi 214122, China;* orcid.org/0000-0001-9953-7681; Email: xpyan@jiangnan.edu.cn

Authors

Tian-Tian Ma − *State Key Laboratory of Food Science and Resources, Jiangnan University, Wuxi 214122, China; International Joint Laboratory on Food Safety and Institute of Analytical Food Safety, School of Food Science and Technology, Jiangnan University, Wuxi 214122, China*

Wen-Chao Deng − *State Key Laboratory of Food Science and Resources, Jiangnan University, Wuxi 214122, China; International Joint Laboratory on Food Safety and Institute of Analytical Food Safety, School of Food Science and Technology, Jiangnan University, Wuxi 214122, China*

Hai-Long Qian − *Institute of Analytical Food Safety, School of Food Science and Technology, Jiangnan University, Wuxi 214122, China;* orcid.org/0000-0001-7554-4115

Shuting Xu − *Institute of Analytical Food Safety, School of Food Science and Technology, Jiangnan University, Wuxi 214122, China*

Cheng Yang − *Institute of Analytical Food Safety, School of Food Science and Technology, Jiangnan University, Wuxi 214122, China*

Complete contact information is available at: https://pubs.acs.org/10.1021/acsmaterialslett.4c00166

Author Contributions

Tian-Tian Ma was responsible for conceptualization, investigation, data curation, validation, and writing (original draft). Wen-Chao Deng was responsible for validation. Hai-Long Qian was responsible for validation. Shuting Xu was responsible for validation. Cheng Yang was responsible for

https://doi.org/10.1021/acsmaterialslett.4c00166
ACS Materials Lett. 2024, 6, 1616−1622

validation. Xiu-Ping Yan was responsible for conceptualization, project administration, writing (review and editing), funding acquisition, and supervision. CRediT: **Tian-Tian Ma** conceptualization, data curation, investigation, validation, writing-original draft; **Wen-Chao Deng** validation; **Hai-Long Qian** validation; **Shuting Xu** validation; **Cheng Yang** validation; **Xiu-Ping Yan** conceptualization, funding acquisition, project administration, supervision, writing-review & editing.

Notes

The authors declare no competing financial interest.

■ ACKNOWLEDGMENTS

This work was supported by the National Natural Science Foundation of China (Nos. 22176073 and 22076066), the Program of "Collaborative Innovation Center of Food Safety and Quality Control in Jiangsu Province".

■ REFERENCES

(1) Wang, Z. H.; Yang, C.; Liu, T. X.; Qian, H. L.; Yan, X. P. Particle Size Regulation of Single-Crystalline Covalent Organic Frameworks for High Performance of Gas Chromatography. *Anal. Chem.* **2023**, *95*, 8145−8149.

(2) Tang, B.; Wang, W.; Hou, H.; Liu, Y.; Liu, Z.; Geng, L.; Sun, L.; Luo, A. A *β*-Cyclodextrin Covalent Organic Framework Used as a Chiral Stationary Phase for Chiral Separation in Gas Chromatography. *Chin. Chem. Lett.* **2022**, *33*, 898−902.

(3) Ma, T. T.; Yang, C.; Qian, H. L.; Yan, X. P. Post-Modification of Covalent Organic Framework for Gas Chromatographic Separation of Isomers. *J. Chromatogr. A* **2022**, *1673*, 463085.

(4) Chen, J.; Huang, Y. N.; Wei, X.; Lei, X. Q.; Zhao, L.; Guan, M.; Qiu, H. D. Covalent Organic Nanospheres: Facile Preparation and Application in High-Resolution Gas Chromatographic Separation. *Chem. Commun.* **2019**, *55*, 10908−10911.

(5) Qian, H. L.; Wang, Z. H.; Yang, J.; Yan, X. P. Building-Block Exchange Synthesis of Amino-Based Three-Dimensional Covalent Organic Frameworks for Gas Chromatographic Separation of Isomers. *Chem. Commun.* **2022**, *58*, 8133−8136.

(6) Yao, L. F.; He, H. B.; Feng, Y. Q.; Da, S. L. HPLC Separation of Positional Isomers on a Dodecylamine-N, N-dimethylenephosphonic Acid Modified Zirconia Stationary Phase. *Talanta* **2004**, *64*, 244−251.

(7) Yang, Y. X.; Bai, P.; Guo, X. H. Separation of Xylene Isomers: A Review of Recent Advances in Materials. *Ind. Eng. Chem. Res.* **2017**, *56*, 14725−14753.

(8) Li, Z.; Ding, X. S.; Feng, Y. Y.; Feng, W.; Han, B. H. Structural and Dimensional Transformations between Covalent Organic Frameworks via Linker Exchange. *Macromolecules* **2019**, *52*, 1257−1265.

(9) Guo, J. X.; Yang, C.; Yan, X. P. Thiol-Ene" Click Synthesis of Chiral Covalent Organic Frameworks for Gas Chromatography. *J. Mater. Chem. A* **2021**, *9*, 21151−21157.

(10) Huang, J. J.; Han, X.; Yang, S.; Cao, Y. Y.; Yuan, C.; Liu, Y.; Wang, J. G.; Cui, Y. Microporous 3D Covalent Organic Frameworks for Liquid Chromatographic Separation of Xylene Isomers and Ethylbenzene. *J. Am. Chem. Soc.* **2019**, *141*, 8996−9003.

(11) Zhang, K.; Cai, S. L.; Yan, Y. L.; He, Z. H.; Lin, H. M.; Huang, X. L.; Zheng, S. R.; Fan, J.; Zhang, W. G. Construction of a Hydrazone-Linked Chiral Covalent Organic Framework-Silica Composite as the Stationary Phase for High Performance Liquid Chromatography. *J. Chromatogr. A* **2017**, *1519*, 100−109.

(12) Zhao, S.; Dong, B.; Ge, R. L.; Wang, C.; Song, X. D.; Ma, W.; Wang, Y.; Hao, C.; Guo, X. W.; Gao, Y. A. Channel-Wall Functionalization in Covalent Organic Frameworks for the Enhancement of CO_2 Uptake and CO_2/N_2 Selectivity. *RSC Adv.* **2016**, *6*, 38774−38781.

(13) Li, D.; Guo, L. J.; Li, F.; Huang, J.; Li, J. H.; Li, M.; Li, C. Q. Synthesis and Catalytic Behavior of Nickel Heterogenized in Covalent Organic Frameworks as Precatalysts in Ethylene Oligomerization. *Micropor. Mesopor. Mater.* **2022**, *338*, 111979.

(14) Chen, G.; Lan, H. H.; Cai, S. L.; Sun, B.; Li, X. L.; He, Z. H.; Zheng, S. R.; Fan, J.; Liu, Y.; Zhang, W. G. Stable Hydrazone-Linked Covalent Organic Frameworks Containing O, N, O′-Chelating Sites for Fe(III) Detection in Water. *ACS Appl. Mater. Inter.* **2019**, *11*, 12830−12837.

(15) Chandra, S.; Roy Chowdhury, D.; Addicoat, M.; Heine, T.; Paul, A.; Banerjee, R. Molecular Level Control of the Capacitance of Two-Dimensional Covalent Organic Frameworks: Role of Hydrogen Bonding in Energy Storage Materials. *Chem. Mater.* **2017**, *29*, 2074−2080.

(16) Guo, H.; Liu, Y. S.; Wu, N.; Peng, L. P.; Wei, X. Q.; Lu, Z. Y.; Yu, Z. G.; Yang, W. A Fluorescent Triazine-Based Covalent Organic Framework as a Highly Sensitive Fluorescent Probe for Fe ions. *New J. Chem.* **2023**, *47*, 1031−1034.

(17) Wang, H.; Li, J. Microporous Metal-Organic Frameworks for Adsorptive Separation of C5−C6 Alkane Isomers. *Acc. Chem. Res.* **2019**, *52*, 1968−1978.

(18) Ma, T. Q.; Li, J.; Niu, J.; Zhang, L.; Etman, A. S.; Lin, C.; Shi, D. E.; Chen, P. H.; Li, L. H.; Du, X.; Sun, J. L.; Wang, W. Observation of Interpenetration Isomerism in Covalent Organic Frameworks. *J. Am. Chem. Soc.* **2018**, *140*, 6763−6766.

(19) Martínez-Abadía, M.; Strutynski, K.; Lerma-Berlanga, B.; Stoppiello, C. T.; Khlobystov, A. N.; Martí-Gastaldo, C.; Saeki, A.; Melle-Franco, M.; Mateo-Alonso, A. *π*-Interpenetrated 3D Covalent Organic Frameworks from Distorted Polycyclic Aromatic Hydrocarbons. *Angew. Chem., Int. Ed.* **2021**, *60*, 9941−9946.

(20) Liang, R. R.; Jiang, S. Y.; A, R. H.; Zhao, X. Two-Dimensional Covalent Organic Frameworks with Hierarchical Porosity. *Chem. Soc. Rev.* **2020**, *49*, 3920−3951.

(21) Zhou, T. Y.; Xu, S. Q.; Wen, Q.; Pang, Z. F.; Zhao, X. One-Step Construction of Two Different Kinds of Pores in a 2D Covalent Organic Framework. *J. Am. Chem. Soc.* **2014**, *136*, 15885−15888.

(22) Liang, R. R.; A, R. H.; Xu, S. Q.; Qi, Q. Y.; Zhao, X. Fabricating Organic Nanotubes through Selective Disassembly of Two-Dimensional Covalent Organic Frameworks. *J. Am. Chem. Soc.* **2020**, *142*, 70−74.

(23) Cheng, J.; Ma, J.; Li, S.; Wang, S.; Huang, C.; Lv, M.; Li, J.; Wang, X.; Chen, L. A Heteropore Covalent Organic Framework for Highly Selective Enrichment of Aryl-Organophosphate Esters in Environmental Water Coupled with UHPLC-MS/MS Determination. *J. Hazard. Mater.* **2024**, *461*, 132613.

(24) Tian, Y.; Xu, S. Q.; Liang, R. R.; Qian, C.; Jiang, G. F.; Zhao, X. Construction of Two Heteropore Covalent Organic Frameworks with Kagome Lattices. *CrystEngComm* **2017**, *19*, 4877−4881.

(25) Ma, T. T.; Yang, C.; Qian, H. L.; Ma, P. M.; Liu, T. X.; Yan, X. P. Trifluoromethyl-Functionalized 2D Covalent Organic Framework for High-Resolution Separation of Isomers. *ACS Appl. Mater. Inter.* **2023**, *15*, 32926−32934.

(26) Lu, T.; Chen, F. W. Multiwfn: A Multifunctional Wavefunction Analyzer. *J. Comput. Chem.* **2012**, *33*, 580−592.

(27) Deng, W. C.; Qian, H. L.; Yang, C.; Xu, S. T.; Yan, X. P. General Two-Step Method for the Fabrication of Covalent-Organic Framework-Bound Open-Tubular Capillary Columns for High-Resolution Gas Chromatography Separation of Isomers. *ACS Appl. Mater. Inter.* **2023**, *15*, 54977−54985.

(28) McReynolds, W. O. Characterization of Some Liquid Phases. *J. Chromatogr. Sci.* **1970**, *8*, 685−691.

(29) Poole, C. F.; Poole, S. K. Characterization of Solvent Properties of Gas Chromatographic Liquid Phases. *Chem. Rev.* **1989**, *89*, 377−395.

(30) Peralta, D.; Chaplais, G.; Simon-Masseron, A.; Barthelet, K.; Pirngruber, G. D. Separation of C-6 Paraffins Using Zeolitic Imidazolate Frameworks: Comparison with Zeolite 5A. *Ind. Eng. Chem. Res.* **2012**, *51*, 4692−4702.

(31) Zhang, Z. Q.; Peh, S. B.; Kang, C. J.; Chai, K. G.; Zhao, D. Metal-Organic Frameworks for C6−C8 Hydrocarbon Separations. *EnergyChem* **2021**, *3*, 100057.

(32) Idrees, K. B.; Kirlikovali, K. O.; Setter, C.; Xie, H.; Brand, H.; Lal, B.; Sha, F.; Smoljan, C. S.; Wang, X.; Islamoglu, T.; Macreadie, L.

https://doi.org/10.1021/acsmaterialslett.4c00166
ACS Materials Lett. 2024, 6, 1616−1622

K.; Farha, O. K. Robust Carborane-Based Metal-Organic Frameworks for Hexane Separation. *J. Am. Chem. Soc.* **2023**, *145*, 23433−23441.
(33) Lin, Y. H.; Yu, L.; Ullah, S.; Li, X. Y.; Wang, H.; Xia, Q. B.; Thonhauser, T.; Li, J. Temperature-Programmed Separation of Hexane Isomers by a Porous Calcium Chloranilate Metal-Organic Framework. *Angew. Chem., Int. Ed.* **2022**, *61*, No. e202214060.
(34) Sholl, D. S.; Lively, R. P. Seven Chemical Separations to Change the World. *Nature* **2016**, *532*, 435−437.
(35) Fang, Z. L.; Zheng, S. R.; Tan, J. B.; Cai, S. L.; Fan, J.; Yan, X.; Zhang, W. G. Tubular Metal-Organic Framework-Based Capillary Gas Chromatography Column for Separation of Alkanes and Aromatic Positional Isomers. *J. Chromatogr. A* **2013**, *1285*, 132−138.
(36) Huang, X. L.; Lan, H. H.; Yan, Y. L.; Chen, G.; He, Z. H.; Zhang, K.; Cai, S. L.; Zheng, S. R.; Fan, J.; Zhang, W. G. Fabrication of a Hydrazone-Linked Covalent Organic Framework-Bound Capillary Column for Gas Chromatography Separation. *SSC plus* **2019**, *2*, 120−128.
(37) Srivastava, M.; Roy, P. K.; Ramanan, A. Hydrolytically Stable ZIF-8@PDMS Core−Shell Microspheres for Gas-Solid Chromatographic Separation. *RSC Adv.* **2016**, *6*, 13426−13432.
(38) Sun, T.; Chen, R. A.; Huang, Q. C.; Ba, M. Y.; Cai, Z. Q.; Chen, H. P.; Qi, Y. H.; Chen, H.; Liu, X. M.; Nardiello, D.; Quinto, M. Efficient Gas Chromatographic Separation of Xylene and Other Aromatic Isomers by Using Pillar[6]arene-Based Stationary Phase. *Anal. Chim. Acta* **2023**, *1251*, 340979.
(39) Tang, W. Q.; Zhao, Y. J.; Xu, M.; Xu, J. Y.; Meng, S. S.; Yin, Y. D.; Zhang, Q. H.; Gu, L.; Liu, D. H.; Gu, Z. Y. Controlling the Stacking Modes of Metal-Organic Framework Nanosheets through Host−Guest Noncovalent Interactions. *Angew. Chem., Int. Ed.* **2021**, *60*, 6920−6925.
(40) Huang, B.; Li, K.; Ma, Q. Y.; Xiang, T. X.; Liang, R. X.; Gong, Y. N.; Wang, B. J.; Zhang, J. H.; Xie, S. M.; Yuan, L. M. Homochiral Metallacycle Used as a Stationary Phase for Capillary Gas Chromatographic Separation of Chiral and Achiral Compounds. *Anal. Chem.* **2023**, *95*, 13289−13296.

https://doi.org/10.1021/acsmaterialslett.4c00166
ACS Materials Lett. 2024, 6, 1616−1622